SUPPLEMENTAL INFORMATION

Supplemental Tables

Table S1. Intracellular distribution*[1] of various proteins and dextran

	Molecular weight [kDa]	Nocodazole (−)		Nocodazole (+)	
		Before NEBD	After NEBD	Before NEBD	After NEBD
GFP	28	eq*[2]	eq	eq*[2]	eq
DYRB-1::GFP	41	C	N	C	N
H2B::GFP	42	N	eq	N	eq
α-Tubulin*[3]	50	C	N*[4]	C	N
DNC-2::GFP	66	C	N	C	N
Texas Red-labeled dextran (70 kDa)	70	C	eq	C	eq
LIS-1::GFP	75	C	N	C	N*[5]
β-Tubulin::GFP	79	C	N*[4]	C	N
DNC-1::GFP	177	C	N	C	N*[5]
NMY-2::GFP	258	C	N	C	N

*[1] N: signal intensity stronger in the nucleus, C: signal intensity stronger in the cytoplasm, eq: no apparent difference in signal intensity between the nucleus and the cytoplasm
*[2] Signal intensity was similar between the nucleus and the cytoplasm but slightly stronger in the nucleus (see text).
*[3] Distribution was analyzed by α-tubulin antibody staining (for other molecules, by live imaging).
*[4] Polymerized tubulin (microtubule) localized to the spindle
*[5] Distribution was not as uniform as with tubulin but was concentrated in the chromosomes instead.

Table S2. *Caenorhabditis elegans* strains used in this study

Strain	Genotype	Provided by	Reference
N2	wild-type		(Brenner, 1974)
AZ244	*unc-119(ed3) III; ruIs57*[*unc-119(+); pie-1p::gfp::tubulin*]	CGC	(Praitis *et al.*, 2001)
JJ1473	*unc-119(ed3) III; zuIs45*[*nmy-2p::nmy-2::gfp; unc-119(+)*] V.	CGC	(Nance *et al.*, 2003)
OD139	*unc-119(ed3) III; ltIs37*[*pie-1p::mCherry::his-58; unc-119(+)*]; *qaIs3502*[*unc-119(+); pie-1p::yfp::lmn-1*]	K. Oegema	(Portier *et al.*, 2007)
mCherry::SP12	*unc-119(ed3) III; ltIs37*[*pie-1p::mCherry::SP12; unc-119(+)*]	J. Audhya	(Green *et al.*, 2008)
WH237	*unc-119(ed3) III; ojIs10*[*gfp::lis-1; unc-119(+)*]	J. White and A. Skop	(Malone *et al.*, 2003)
WH257	*unc-119(ed3) III; ojIs5*[*pie-1p::gfp::dnc-1; unc-119(+)*]	CGC	(Zhang *et al.*, 2008)
WH258	*unc-119(ed3) III; ojIs57*[*pie-1p::gfp::dnc-2; unc-119(+)*]	CGC	(Zhang *et al.*, 2008)
CAL0135	*unc-119(ed3) III; wjIs15*[*unc-119(+); pie-1p::gfp::dyrb-1*]		(Kimura and Kimura, 2011)
CAL0361	*unc-119(ed3) III;* [*unc-119(+); pie-1p::gfp*]		This study
CAL0451	*unc-119(ed3) III; ltIs37*[*pie-1p::mCherry::SP12; unc-119(+)*]; *ruIs57*[*unc-119(+); pie-1p::gfp::tubulin*]		This study
CAL0461	*unc-119(ed3) III; ltIs37*[*pie-1p::mCherry::his-58; unc-119(+)*]		This study
CAL0491	*unc-119(ed3) III; ltIs37*[*pie-1p::mCherry::his-58; unc-119(+)*]; *ruIs57*[*unc-119(+); pie-1p::gfp::tubulin*]		This study

CGC: *Caenorhabditis* Genetics Center, University of Minnesota, MN, USA

Table S3. Sequences of the primers used for RNAi

Gene	Primer	Oligo (5′→3′)	Reference
dhc-1 (T21E12.4)	T3	AATTAACCCTCACTAAAGGCCTTTCCTTCCTGGGTCTTC	Phenobank
	T7	TAATACGACTCACTATAGGCAAGGAAGGAGCTCAACGAC	
ran-1 (K01G5.4)	T3	AATTAACCCTCACTAAAGGTTAAAGATCATCGTCGTCATCTG	(Askjaer *et al.*, 2002)
	T7	TAATACGACTCACTATAGGATGTCTGGTGGAGACGGCATCC	
lmn-1 (DY3.2)	T3	AATTAACCCTCACTAAAGGAACCTCGTCGATTCCAACTG	Phenobank
	T7	TAATACGACTCACTATAGGAAATCGAAGAGATGCGTGCT	
ran-3 (C26D10.1)	T3	AATTAACCCTCACTAAAGGATTGGCGATCGAGTTTTGTC	(Askjaer *et al.*, 2002)
	T7	TAATACGACTCACTATAGGAACAATCGAATTGGCTACCG	

Supplemental Figures

Figure S1. Tubulin accumulates in the nascent spindle region of the *Caenorhabditis elegans* 1-cell-stage embryo.
Immunofluorescence of a 1-cell-stage embryo of N2 (wild-type) strain treated with 10 μg/ml nocodazole [noc(+)]. Z-projections of embryos stained for α-tubulin (green), and DNA (DAPI, blue) are shown. In this figure and all other figures, the anterior side is to the left and the posterior side is to the right. Scale bar: 5 μm.

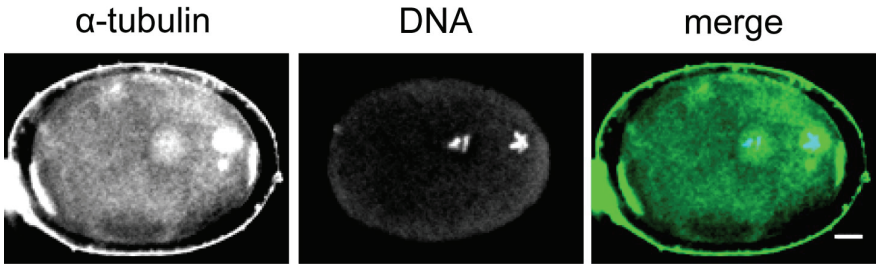

Figure S2. Timing of CeNEBD processes: free H2B exit, dextran entry, and LIS-1 entry.
(A) Validation of free H2B exit from the nucleus as a marker for CeNEBD. To compare the timing of histone H2B exit and 70-kDa dextran entry into the nuclear/nascent spindle region, Texas Red-labeled 70-kDa dextran was injected into H2B::GFP-expressing worms and the embryos were observed. (B) LIS-1 enters the nuclear region not before CeNEBD. The 70-kDa dextran was injected into LIS-1::GFP-expressing worms and the embryos were observed. Single optical sections along the equator of the nucleus of a 1-cell-stage embryo are shown. M: male pronucleus, F: female pronucleus. Scale bars: 5 μm.

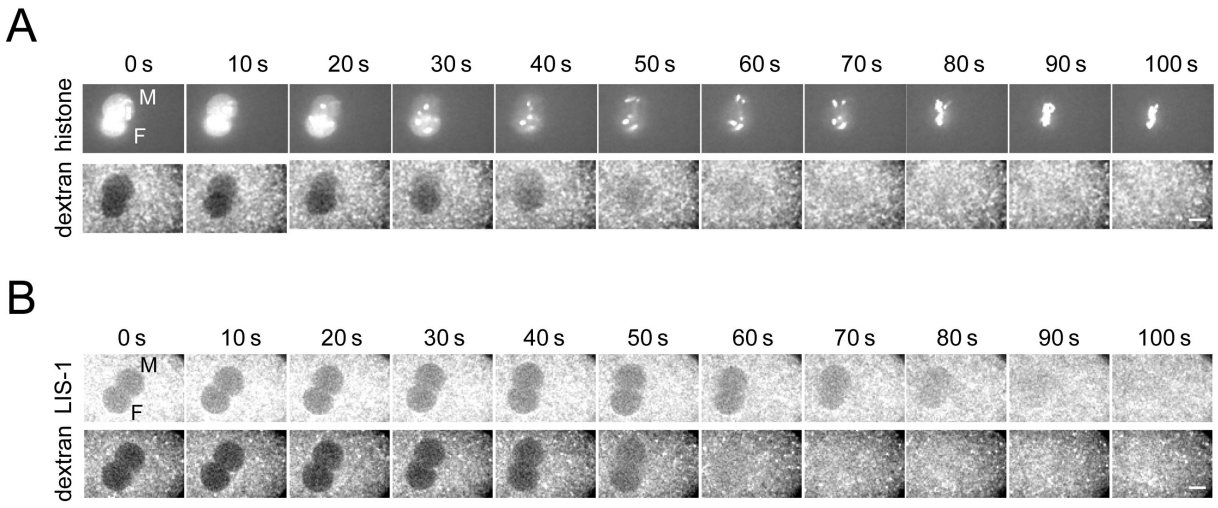

Figure S3. *lmn-1* (RNAi) induces untimely permeabilization of the nuclear envelope.
(A) The SP12::mCherry-labeled nuclear envelopes appeared intact upon the untimely permeabilization in the *lmn-1* (RNAi) embryo but disappeared before spindle formation. Time-lapse imaging of the wild-type (control) and *lmn-1* (RNAi) embryos expressing β-tubulin::GFP and SP12::mCherry. The single confocal sections of the selected time points during and after the cortical ruffling stage are shown for each embryo. $t = 0$ s indicates the completion of the cortical ruffling. Upon the untimely accumulation of tubulin (arrow) in the *lmn-1* (RNAi) embryo, the SP12::mCherry-labeled nuclear envelope appeared intact but the SP12 signal was no longer detected at the nuclear/spindle envelope after the cortical ruffling stage. Scale bars: 5 μm.
(B) The entry of 70-kDa dextran into the nuclear region also occurred early in *lmn-1* (RNAi). Texas-Red-labeled 70-kDa dextran was injected into H2B::GFP- or β-tubulin::GFP-expressing worms, and the embryos were observed during and after the cortical ruffling stage. $t = 0$ s indicates the completion of the cortical ruffling. The 70-kDa dextran entered the nuclear region during the cortical ruffling (arrow), concurrent with the entry and the accumulation of free tubulin in the nuclear region of the *lmn-1* (RNAi) embryos. In the control embryos, the 70-kDa dextran entered the nascent spindle region after cortical ruffling (arrow), concurrent with the diffusion of free histones into the cytoplasm. We do not present images during the cortical ruffling in the controls, in which the permeabilization occurred after the cortical ruffling. Scale bars: 5 μm.

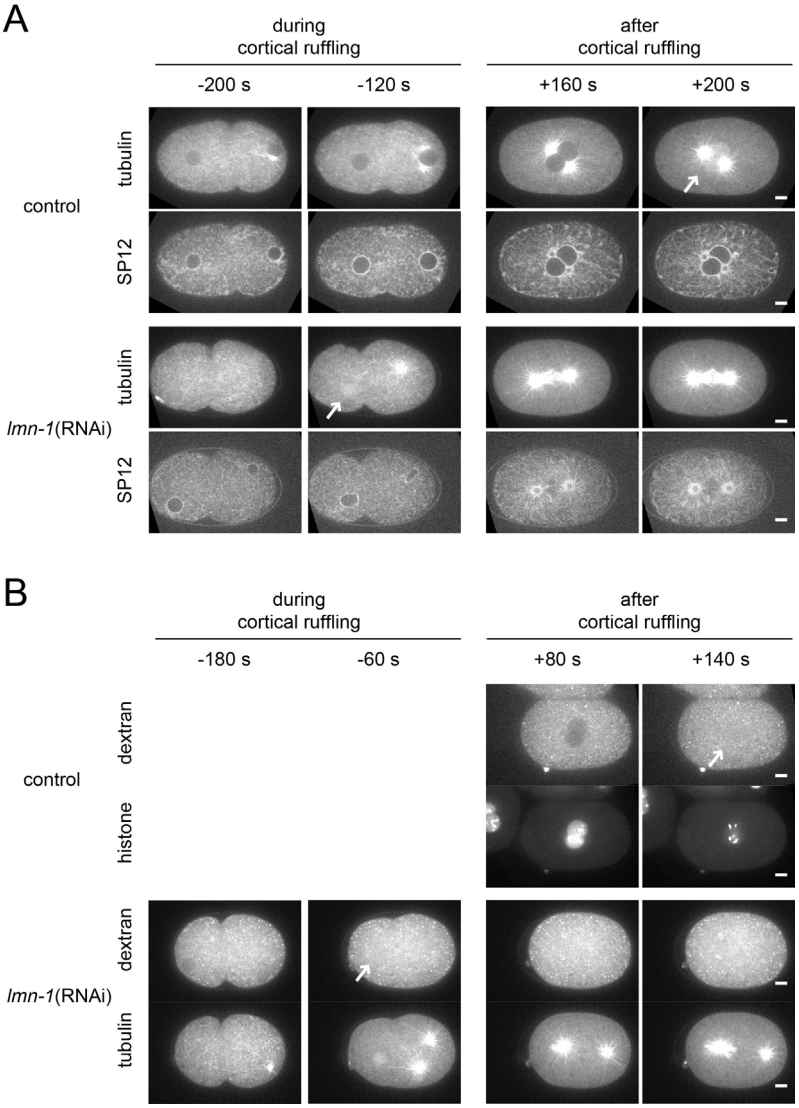

Figure S4. SP12::mCherry-labeled nuclear envelope appeared intact in the *ran-1* (RNAi) embryos.
Time-lapse imaging of wild-type (control) (A), *ran-1* (RNAi) (B), and *ran-3* (RNAi) embryos expressing β-tubulin::GFP and SP12::mCherry, with 10 μg/mL nocodazole. The single confocal sections immediately before and after CeNEBD are shown for each embryo. Scale bars: 5 μm.

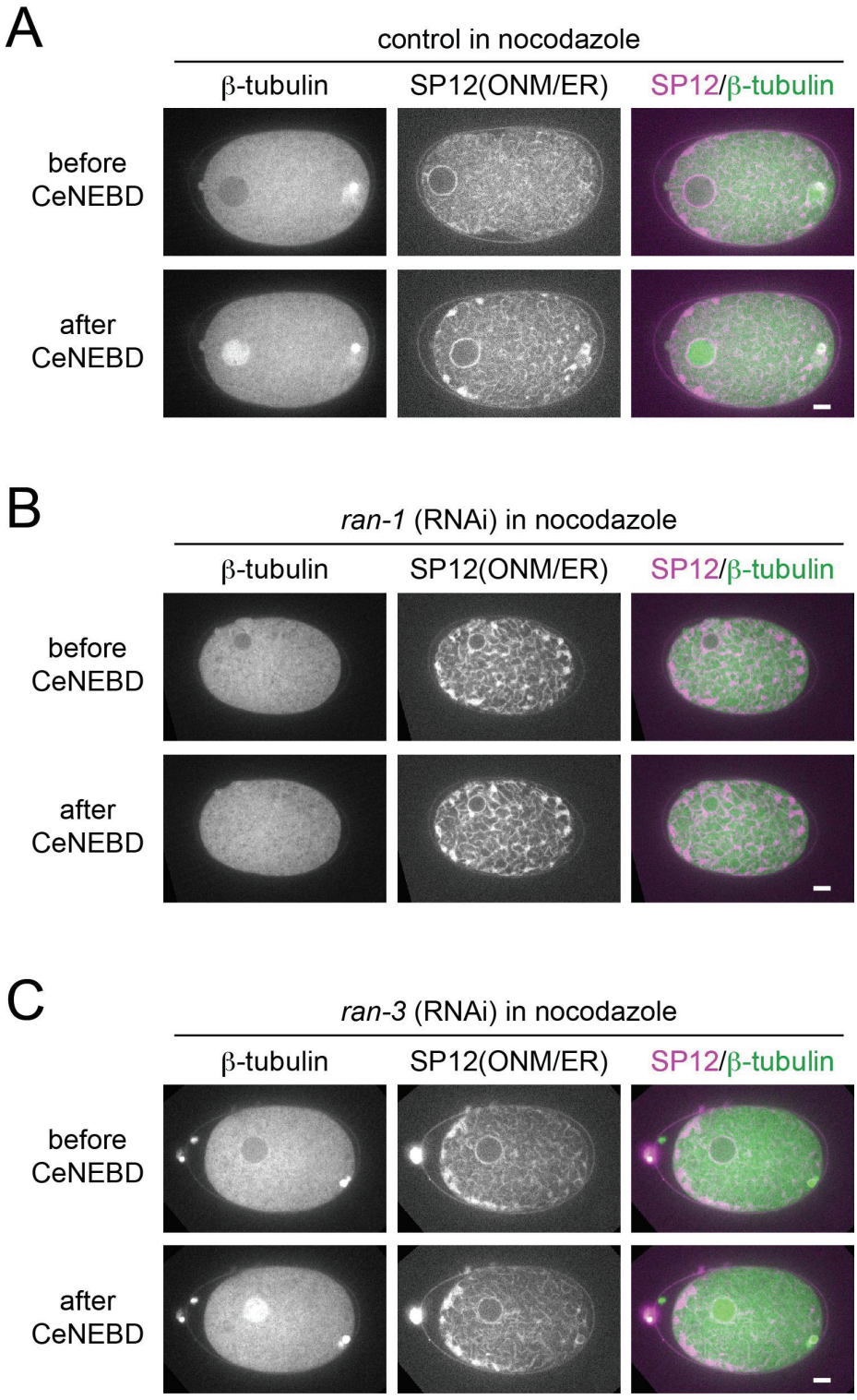

Figure S5. Condensed chromosomes did not prevent tubulin accumulation in the *ran-1* (RNAi) embryos.
Time-lapse imaging of the *ran-1* (RNAi) embryo expressing β-tubulin::GFP and H2B::mCherry, with 10 μg/mL nocodazole. The single confocal sections before and after CeNEBD are shown. The insets in the lower panels are ×5 magnifications of the nuclear regions (arrows). The chromosome condensation was defective in *ran-1* (RNAi), as previously reported. However, the decondensation of chromosome was unlikely the cause of the defect in tubulin accumulation because there was no apparent difference in tubulin accumulation whether the regions did or did not contain the chromosomes. Scale bars: 5 μm.

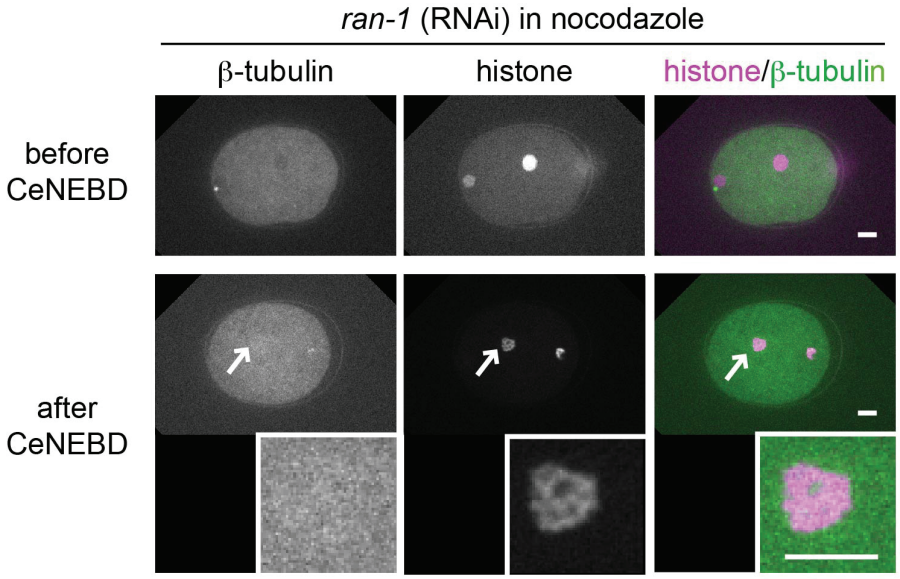

Figure S6. Fitting of the FRAP data to exponential curves.
A plot of the normalized mean fluorescence intensity (gray solid square) is shown along with the fitted exponential curve (black lines in the upper panels). In the lower panels, residual differences between the raw data and the fit curve are shown. Normalized fluorescence intensity and residual differences (A) inside the nascent spindle region in control cells, (B) in the cytoplasmic region of control cells, (C) in the nascent spindle region of *ran-1* (RNAi) cells, and (D) in the cytoplasmic region of *ran-1* (RNAi) cells.

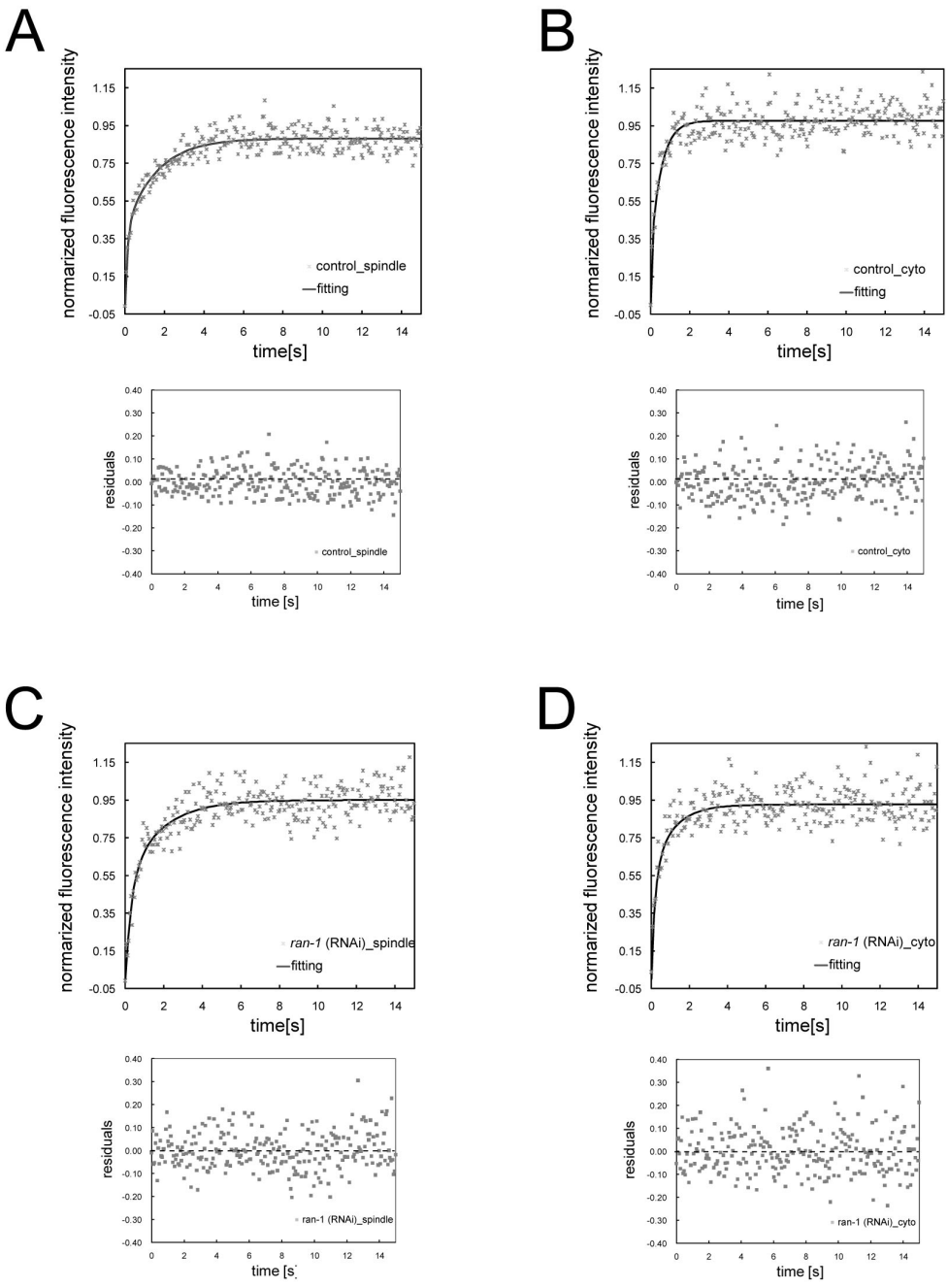

Figure S7. Evaluation of the photobleached area along the axis perpendicular to the confocal plane in Figure 6C.
Fixed 4-cell-stage embryos were stained with an anti-α-tubulin antibody and photobleached. Images before (a and b) and immediately after photobleaching the cytoplasm (c and d) are shown. a and c show the confocal section where the bleaching laser was illuminated. In b and d, images are the virtual cross-section along the Z-axis over 16 μm corresponding to the length (top to bottom) of the embryo. The geometry of the bleached region from the view of the XY plane is shown in a single confocal section (c, arrowhead); the geometry of bleach from the view of the XZ plane is also shown (d, bi-directed arrow). The box on the right of each image denotes the intensity range. Scale bars: 5 μm.

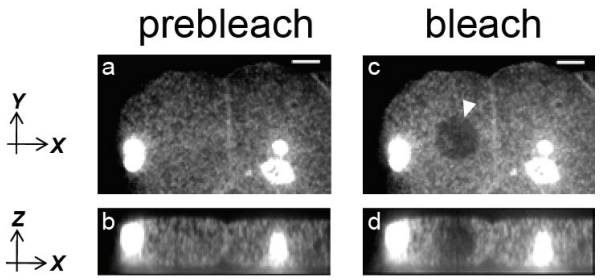

REFERENCES

Askjaer, P., Galy, V., Hannak, E., and Mattaj, I.W. (2002). Ran GTPase cycle and importins alpha and beta are essential for spindle formation and nuclear envelope assembly in living Caenorhabditis elegans embryos. Mol Biol Cell *13*, 4355-4370.

Brenner, S. (1974). The genetics of Caenorhabditis elegans. Genetics *77*, 71-94.

Green, R.A., Audhya, A., Pozniakovsky, A., Dammermann, A., Pemble, H., Monen, J., Portier, N., Hyman, A., Desai, A., and Oegema, K. (2008). Expression and imaging of fluorescent proteins in the C. elegans gonad and early embryo. Methods Cell Biol *85*, 179-218.

Kimura, K., and Kimura, A. (2011). Intracellular organelles mediate cytoplasmic pulling force for centrosome centration in the Caenorhabditis elegans early embryo. Proc Natl Acad Sci U S A *108*, 137-142.

Malone, C.J., Misner, L., Le Bot, N., Tsai, M.C., Campbell, J.M., Ahringer, J., and White, J.G. (2003). The C. elegans hook protein, ZYG-12, mediates the essential attachment between the centrosome and nucleus. Cell *115*, 825-836.

Nance, J., Munro, E.M., and Priess, J.R. (2003). C. elegans PAR-3 and PAR-6 are required for apicobasal asymmetries associated with cell adhesion and gastrulation. Development *130*, 5339-5350.

Portier, N., Audhya, A., Maddox, P.S., Green, R.A., Dammermann, A., Desai, A., and Oegema, K. (2007). A microtubule-independent role for centrosomes and aurora a in nuclear envelope breakdown. Dev Cell *12*, 515-529.

Praitis, V., Casey, E., Collar, D., and Austin, J. (2001). Creation of low-copy integrated transgenic lines in Caenorhabditis elegans. Genetics *157*, 1217-1226.

Zhang, H., Skop, A.R., and White, J.G. (2008). Src and Wnt signaling regulate dynactin accumulation to the P2-EMS cell border in C. elegans embryos. J Cell Sci *121*, 155-161.